End ring inductance of a squirrel-cage induction motor using 2D and 3D finite element methods

R. De Weerdt K. Hameyer R. Belmans

Dept. ESAT, Research Group ELEN
Kard. Mercierlaan 94, 3001 LEUVEN, BELGIUM
Tel. + 32 (0) 16 32 10 20 Fax + 32 (0) 16 32 19 85

Abstract - **The paper describes the calculation of the inductance of the end ring of a squirrel-cage induction motor using finite elements. The inductance values are obtained using 2D and 3D finite elements and the results are compared with an analytical solution. The ring inductance is split into a leakage component and a mutual component describing the coupling between end ring and end winding. The variation of both components at different load situations is described. It is shown that the ring inductance has significant influence at the locked rotor. This influence is shown by calculations of the locked rotor current with and without inclusion of the end ring inductance using a 2D finite element method. Comparisons with measurements are given.**

I. Introduction

Over the last decades, a lot of effort is made in calculating squirrel-cage induction motors using finite elements. The finite element model used in general is a two dimensional and describes a part of the cross-section of the motor. No three dimensional models consisting of both iron core and end section are considered due to the following reasons. To obtain an accurate solution, a dense mesh is required in the airgap region of the induction motor. Since the induction motor has a narrow airgap, the three dimensional model must also have this dense element distribution leading to a large number of elements and resulting in unacceptable computational costs.

The inclusion of both saturation and eddy currents simultaneously is essential for the induction motor analysis. This requires a transient solution [1] or is approximated using a time-harmonic solution in combination with a modified magnetisation curve (method of effective reluctivities) [2,3] or a combination of static and time-harmonic solutions [4,5].

To obtain a realistic result, the inclusion of the motor end effects is essential. The motor end effects can be split into four components: the stator end winding resistance and inductance and the end ring resistance and inductance. Motors with copper cage have bars that are somewhat longer than the iron core, yielding an additional impedance that has a totally different behaviour with respect to current redistribution due to skin effect. For the inductance components, only the leakage part of the end winding or end ring inductance is important. The mutual inductance between end ring and stator end winding is part of the magnetising inductance. However, it can be neglected in practice. This coupling mainly takes place in air and therefore, it is very weak. The end effect parameters can be incorporated in the two dimensional problem as lumped parameters. This results in a set of equations containing the finite element problem and a number of circuit equations, describing the circuit external to the two-dimensional model. Analytical and empirical formulae exist for the end effect parameters, but the origin of these formulae is not always clear. Furthermore, the derivation of such empirical formulae is both costly and time-consuming since they require full size prototyping and measurements. Due to the influence of saturation on the parameters, all tests have to be performed at rated voltage. This is extremely difficult when looking at the locked rotor test. Therefore, a calculation of the motor end effect parameters, rather than determining them by measurements is of economical interest to the industry. During load situations, the end ring resistance has the most significant influence on the motor behaviour. Although the resistance of a ring segment R_r is much smaller than the bar resistance R_b (about 1 % of the bar resistance) its influence can be up to 20 to 30 % as shown by

$$R_{eqb} = R_b + \frac{R_r}{2\sin^2\left(\frac{p\pi}{N}\right)} \tag{1}$$

The equivalent bar resistance R_{eqb} is the resistance to be used to include the Joule-losses in the ring when calculating the losses from the bar currents. N is the number of rotor bars and p is the number of pole pairs. Since the stator end winding inductance is difficult to calculate analytically, most authors introduce some empirical formulae [6]:

$$X_s = 0.4\mu_0 f \frac{w^2}{p} \Lambda_s \tag{2}$$

Equation (2) expresses the end winding reactance X_S as a function of the supply frequency f, the number of windings in series w, the number of pole pairs p, and the parameter Λ_S. Λ_S is proportional to the length of the end winding and is determined experimentally for various types of windings. In the classical analysis, the ring inductance is often said to be negligible. Since the end winding reactance of the stator is determined empirically, it is difficult or either impossible to confirm this statement. Furthermore, the influence of the end ring may or may not be included in Λ_S. The reason why the ring inductance is said to be negligible might be found when (1) is evaluated to determine the influence of the ring inductance in comparison with the bar inductance. In this case, one indeed finds a very small influence of the ring inductance. The motor end ring is mainly surrounded by air, while the bars are embedded in laminated iron. Therefore, the inductance of a ring segment is much smaller than one percent of the bar inductance. Especially during rated load conditions, when

0-7803-3008-0/95 $4.00 © 1995 IEEE

even the bar reactance is small in comparison with the bar resistance, no distinct influence of the end ring inductance is found. However, unlike the influence of the ring resistance, the influence of the ring inductance is not similar for all load points. For the locked rotor operation, only the bar leakage has to be considered and not the full bar inductance. The different leakage components (slot leakage, zigzag leakage, airgap leakage) are much smaller than the bar inductance since they describe flux linkages located in air and not in laminated iron. Therefore, it is premature to state that the ring inductance can be neglected.

Using a three dimensional finite element solution, the end winding leakage, the end ring leakage and the coupling between both stator and rotor end effects can be calculated for different load conditions. The importance of these parameters can be determined and they can be placed at the correct locations in the coupled finite-element - circuit model. The influence of the ring inductance is then determined by including or neglecting it during the calculations and by comparing results.

II. Analytical End Ring Inductance Calculation

Describing the influence of the end ring inductance, in [7] the following expression is found:

$$L_e = \mu_0 \frac{N}{3p}\left(\frac{1}{3}(l_b - l_i) + k\tau'\right) \tag{3}$$

Where l_b is the bar length, l_i is the length of the iron lamination, τ' is the pole pitch diameter in the middle of the ring, k = 0.18 for p = 1 and k = 0.36 for p > 1. (3) expresses the influence of the end ring *per bar*. To compare the analytical formula with the 2D and 3D calculations, expression (3) is divided by $2\sin^2\left(\frac{p\pi}{N}\right)$ to refer it to the ring (as in (1)) and multiplied by N in order to obtain an expression for the ring inductance L_r:

$$L_r = \frac{\mu_0 N^2\left(\frac{1}{3}(l_b - l_i) + k\tau'\right)}{6p * \sin^2\left(\frac{p\pi}{N}\right)} \tag{4}$$

The value of the ring inductance of the motor under consideration using (4) is $L_r = 0.84\ \mu H$.

III. Two Dimensional End Ring Inductance Calculation

For the 2D finite element calculation, a model is made of an axial cross-section of the motor end region (figure 1). As an example, a 400 kW traction motor is modelled. The accurate modelling of the cross-section is difficult to obtain since it contains a number of different materials with different, often unknown and generally anisotropic magnetic properties. Also for the correct modelling of the boundary between bearings and frame or bearings and shaft questions arise whether to model them as good or bad magnetically permeable. To overcome these questions, a number of models are built using different boundary conditions and materials in order to find the influence of each component of the end region.

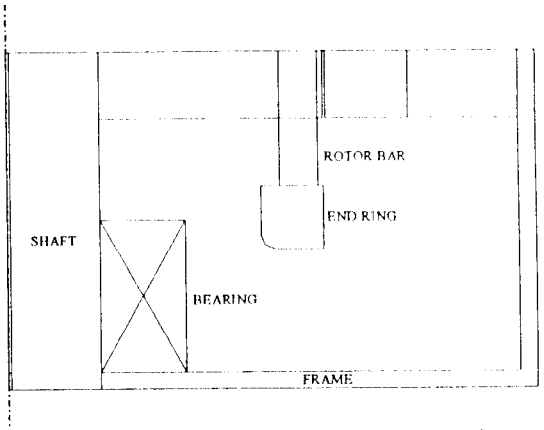

Fig. 1: Axial cross-section of a squirrel-cage induction motor end region

This is similar to the approach used in [8] where two extreme situations are considered, one where the boundary of the frame, bearing and shaft is considered to be a flux line, the other where the boundary is considered perfectly magnetically permeable. The finite element problem is described as axisymmetric. A unit current is considered to flow in the end ring. The problem is defined as time harmonic, neglecting saturation. The following figures show flux plots for some of the models taking different boundary conditions and material properties into account (figures 2 to 4).

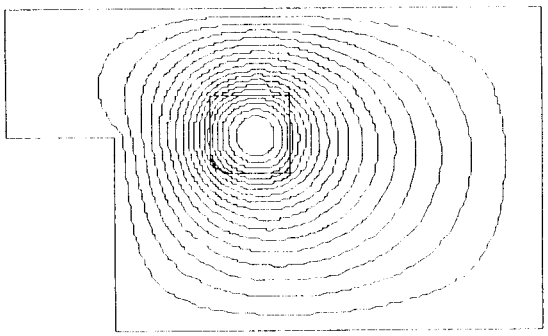

Fig. 2: Only the air around the end ring is modelled and considered to be a flux line

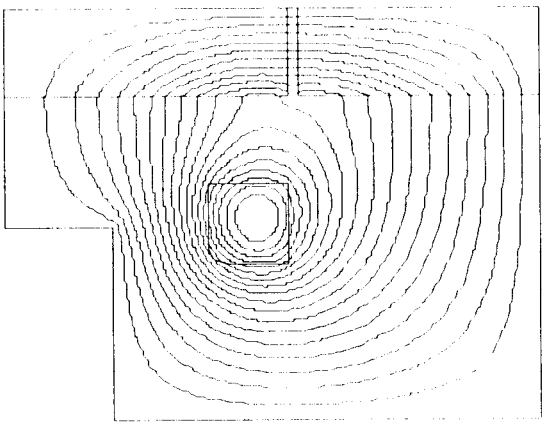

Fig. 3: Stator and rotor iron included

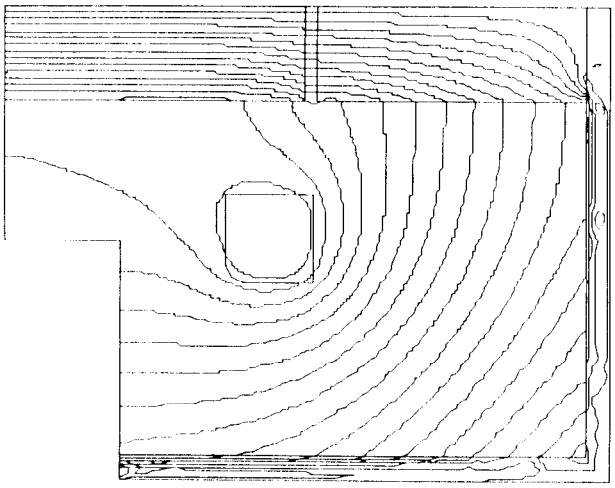

Fig. 4: Frame of the motor in cast iron, shaft and bearings magnetically infinitely permeable.

The inductance values obtained from figures 2 to 4 are 0.35 μH, 0.42 μH and 0.94 μH. When all boundaries are considered to be magnetically conducting, only the air surrounding the ring has to be modelled (figure 5).

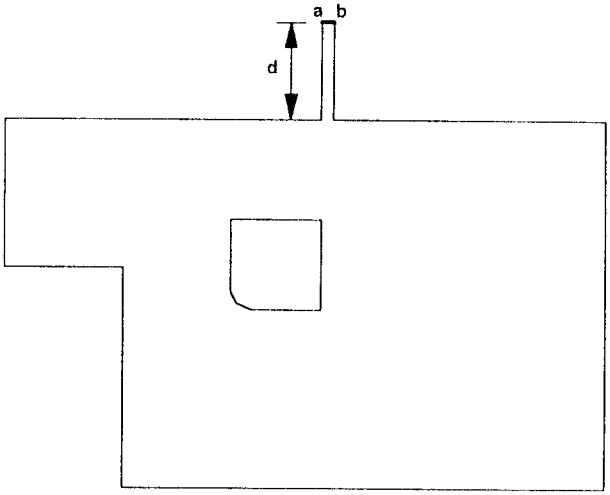

Fig. 5: Outline of the finite element model to examine the magnetically conducting situation

Line piece $\overline{ab}$ in figure 5 is constrained to be a flux line. It is necessary to have at least one piece of the boundary considered to be a flux line, if not, there exists no physical solution for the problem. Examining the solutions of this model, a large variation in the inductance is found when distance the d is altered. The modelling requires that d is equal to half the core length. Only then $\overline{ab}$ is a realistic flux line. The inductance value obtained in this case is 13.05 μH. This is a large difference compared to the other extreme situation where all material boundaries are considered to be a flux line (figure 2). Therefore, from the 2D approach it is not obvious which value for the ring inductance has to be used as lumped parameter in the coupled finite element - circuit model.

The 2D approach has some additional drawbacks.

First, the correct excitation of the ring via the bars can not be accounted for in a 2D axisymmetric approximation. Therefore, the inductance of the bar ends outside the iron core, are not included in the calculations.

Second, by exciting the ring in an axisymmetric problem definition, a flux through the shaft is introduced. In reality, this flux does not exist. Furthermore, since only the leakage part of the ring inductance is needed, the coupling with the stator end winding has to be considered. It is obvious that all flux through the frame links both end ring and end windings. Therefore, it is part of the mutual inductance and not part of the leakage components. To conclude, separating the mutual and leakage components can only be done using a 3D approach.

IV. Three Dimensional End Ring Inductance Calculation

A. Three dimensional model

The motor modelled consists of 48 stator slots and 40 rotor slots. The stator has a two layer winding short-pitched by two slots. The motor has open rotor slots. Figure 6 shows the cross-section of one pole together with the winding layout.

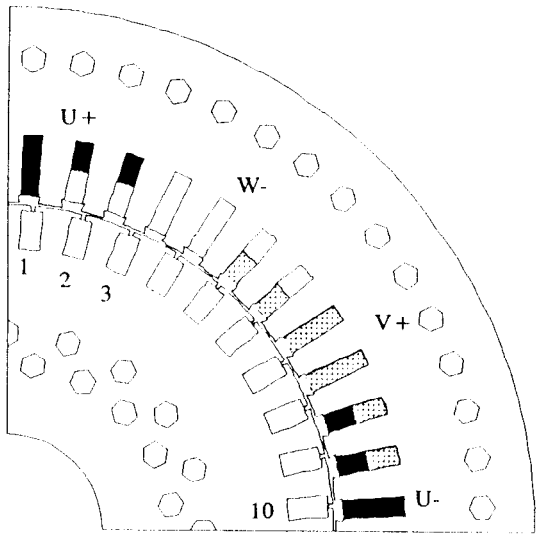

Fig. 6: Outline and winding layout of a cross-section of the motor under consideration

The 3D model is built using an extrusion based mesh generator [9]. Due to symmetry, only one fourth of one end region has to be modelled. The 3D model consists of a material mesh and a set of coil meshes required for the currents. Both meshes are generated separately allowing a different extrusion direction for material mesh and coil meshes. The material mesh can be built by rotating a base plan similar to figure 1 around the center line of the shaft or by shifting a base plan similar to figure 6 in the axial direction. All outlines required in the material mesh have to be present in the base plane. Figure 7 shows the material mesh when the extrusion is performed in axial direction. From this figure it can be seen that a part of the iron core is modelled as well.

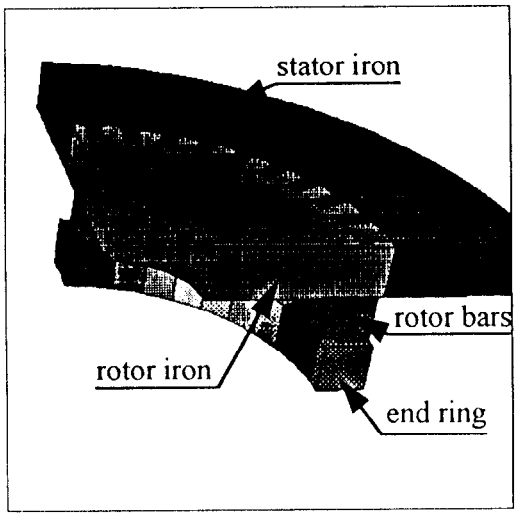

Fig. 7: 3D material mesh built by extrusion in axial direction

The stator end winding is not incorporated in the material mesh. The end winding is modelled as a set of current driven coils in air. This is feasible since current redistribution due to skin effect is negligible in the stranded stator end winding. In the end ring and the rotor bars, skin effect cannot be neglected. Therefore, they are incorporated in the material mesh. Figure 8 shows part of the material mesh (end ring and bar ends) generated by rotating a base plane around the center line of the shaft together with the coil meshes describing the stator end winding.

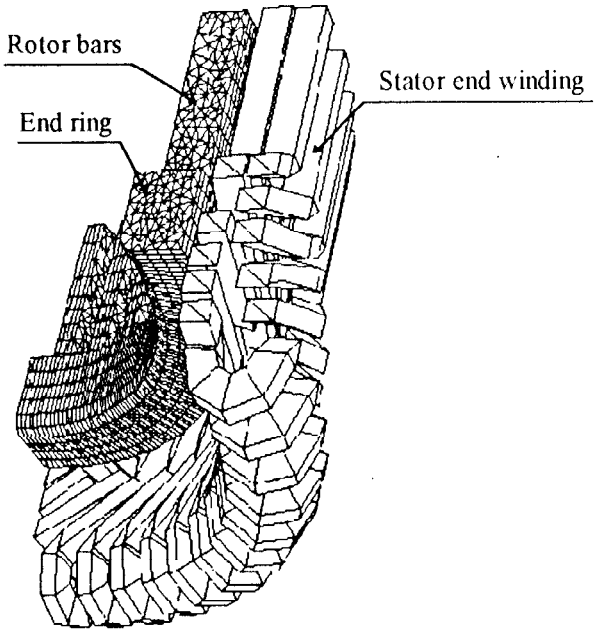

Fig. 8: Material mesh of end ring and bar ends and coil meshes of the stator end winding

Referring to figure 8, it is obvious that the generation of the stator end winding coils requires a more complex extrusion compared to the material mesh modelling. Therefore, the building of such complex models using extrusion techniques is only possible if material and coil meshes can be built separately. Because the stator end winding is not modelled in the material mesh, the coil meshes have to represent the actual end winding geometry as accurate as possible. This is not required for the coil meshes used for the excitation of the end ring and bar ends. Because the end ring and bar ends are modelled in the material mesh, the coil meshes for exciting them only have to be inside the materials and provide a path for the current to flow. The current occupies the full material available taking skin effect into account.

B. Excitations

Both stator and rotor coils are defined as current driven. In the 3D model 9 full ring segments and 2 half segments are present (figures 6,7). Therefore, 11 rotor coils are required for the current excitation. The stator winding is represented by 22 current driven coils. Only 2 end winding coils are completely inside the model, the other 20 coils are cut off at the boundaries of the model (figure 8). Figure 9 shows some of the end winding coils used for the end winding excitation.

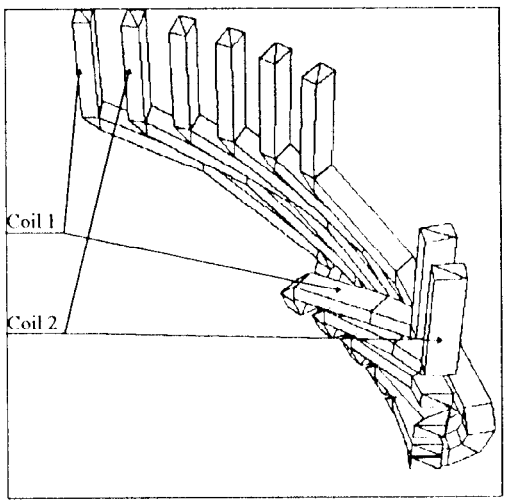

Fig. 9: Coil meshes representing the end winding model

Figure 9 shows the two end winding coils that are completely inside the model (coil 1 and coil 2) together with three other coils that are cut off at the boundary of the model. When referring to the cross-section of figure 6, coil 1 occupies the upper half of the first stator slot (the slot in the upper left corner) and the lower half of slot eleven, coil 2 occupies the upper half of the second slot and the lower half of slot twelf. In the real motor, each of the stator coils contains four turns.

The currents for both rotor and stator coils are obtained from a two dimensional finite element analysis. This analysis is performed at various slip values. Figures 10 to 12 show the currents in the three stator phases, the currents in the rotor bars and ring segments as phasors for the different slip values. The numbering of the bars

is given in figure 6. Ring segment 2 is the ring segment between bars 1 and 2. For clarity, the stator currents are enlarged 10 times.

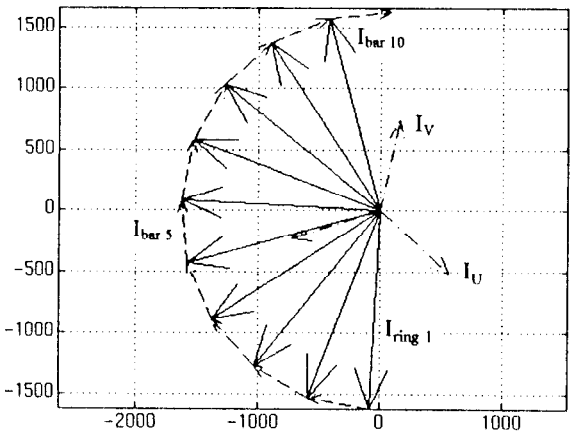

Fig. 10: Phasor diagram of stator- ring- and bar currents (s = 0.34%)

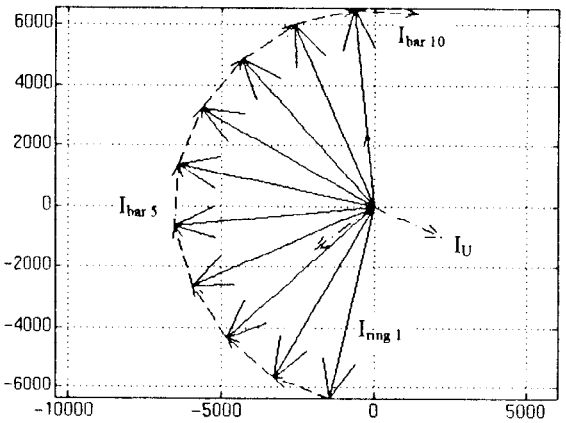

Fig. 11: Phasor diagram of stator- ring- and bar currents (s = 1.42%)

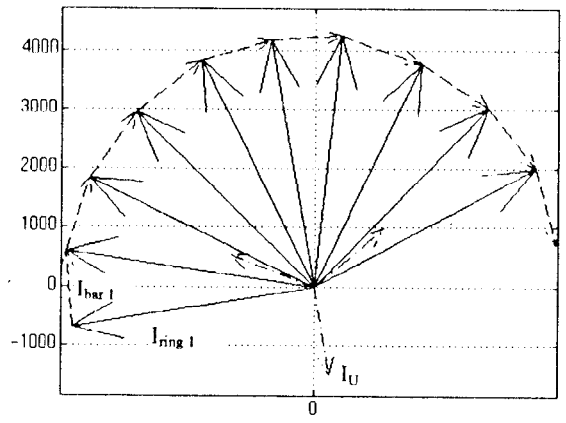

Fig. 12: Phasor diagram of stator- ring- and bar currents (s = 1)

The currents in figure 12 are calculated with reduced supply voltage in order to obtain the rated stator current at standstill. From the figures 10 to 12, an increasing phase shift between the stator mmf and the rotor mmf is noticed. At standstill (figure 12) the stator mmf is approximately 180° shifted with respect to the rotor mmf.

The three dimensional problem is defined as time-harmonic, neglecting saturation in the iron core. The currents in each of the 33 coils is defined by it's amplitude and phase angle according to figures 10 to 12.

C. Calculation of inductances

For each of the slip values, five inductance values are be calculated:

L_r	end ring inductance
L_s	end winding inductance
M	mutual inductance between end ring and end winding
$L_{\sigma r}$	end ring leakage inductance
$L_{\sigma s}$	end winding leakage inductance

The inductances are calculated based on the stored energy in the model [10]. To determine both leakage components and the mutual inductance three problems have to be solved: one having only the stator coils excited, one having only the rotor coils excited and one with both stator and rotor coils excited. Considering the stored energy in these problems to be W_{m1}, W_{m2} and W_{m3}, the following equations are valid:

$$W_{m1} = \frac{m}{2}\frac{1}{8} L_s i_1^2$$

$$W_{m2} = \frac{1}{2*4} L_r i_r^2 = \frac{m}{2}\frac{1}{8} L'_r (i'_r)^2 \qquad (5)$$

$$W_{m3} = \frac{m}{2}\frac{1}{8} L_s i_1^2 + \frac{m}{2}\frac{1}{8} L'_r (i'_r)^2 \pm \left(\frac{m}{2}\frac{1}{8} M_{rs} i_1 i'_r + \frac{m}{2}\frac{1}{8} M_{sr} i_1 i'_r \right)$$

where

L'_r: end ring inductance referred to the stator,
i_r: ring current,
i'_r: ring current referred to the stator,
i_1: stator current,
M_{rs}, M_{sr}: mutual inductance between stator end winding and rotor end ring,
m: number of phases (m = 3).

Since the rotor values are referred to the stator, $M_{rs} = M_{sr} = M$. The value W_{m3} is less than $W_{m1} + W_{m2}$ (the negative sign has to be applied in the expression for W_{m3}) if the flux caused by the rotor excitations opposes the stator flux. If the rotor flux supports the stator flux, W_{m3} is larger than $W_{m1} + W_{m2}$. Under normal conditions, the rotor flux opposes the stator flux, resulting in $W_{m3} < W_{m1} + W_{m2}$ (figure 11). The division by eight or four in (5) takes into account that only one fourth of one end region or one fourth of one end ring is modelled.

In the case only the mutual inductance has to be calculated, it is sufficient to solve two problems. The first with the rotor flux

opposing the stator flux, and the second with the rotor flux supporting the stator flux. The difference of both stored energy values is only a function of the mutual inductance and the applied currents [10]. Introducing the end ring leakage referred to the stator, $L'_{\sigma r}$, the different inductances can be calculated from

$$
\begin{aligned}
L_s &= W_{m1}\frac{2}{m}\frac{8}{i_1^2} & L_{\sigma s} &= L_s - M \\
L_r' &= W_{m2}\frac{2}{m}\frac{8}{(i_r')^2} & L'_{\sigma r} &= L'_r - M \\
L_r &= W_{m2}\frac{2*4}{i_r^2} & L_{\sigma r} &= L_r\frac{L'_{\sigma r}}{L'_r} = L_r\left(1-\frac{M}{L'_r}\right) \\
M &= (W_{m3} - W_{m1} - W_{m2})\frac{8}{3 i_1 i_r'}
\end{aligned}
\qquad (6)
$$

Because the three dimensional calculations performed are linear calculations, the number of calculations is reduced. The calculations with only the rotor- or only the stator coils excited, are performed only once with a unit current. From both calculations, L_s and L_r are obtained. Using (5), the values for the stored energy W_{m1} and W_{m2} for the actual currents i_1 and i_r (or i'_r) are obtained. Therefore, for each slip value, only one additional calculation is required, with both rotor and stator coils excited.

D. Results

The results of the calculations of the different inductance components are shown in table 1. It is seen from table 1 that both mutual and leakage components are strongly slip dependent.

Table 1: Calculated inductance components at different slip values

Inductance	slip [%]		
[mH]	0.34	1.42	100
L_s	0.49	0.49	0.49
L_r'	0.46	0.46	0.46
L_r	0.65e-3	0.65e-3	0.65e-3
M	0.13	0.19	0.21
$L_{\sigma r}'$	0.33	0.30	0.25
$L_{\sigma r}$	0.47e-3	0.42e-3	0.35e-3
$L_{\sigma s}$	0.36	0.30	0.28

It can be stated that during no-load operation, the full stator end winding inductance L_s acts as leakage. Therefore, the end winding leakage inductance $L_{\sigma s}$ varies from 0.49 mH (at no-load) to 0.28 mH (at standstill). The mutual inductance increases when the slip increases, the end winding leakage inductance and the end ring leakage inductance decrease with the same amount. Furthermore, the end ring leakage referred to the stator, $L'_{\sigma r}$ is found to be of the same magnitude as the end winding leakage inductance $L_{\sigma s}$. This already is an indication that the influence of the end ring leakage is not negligible in all load situations.

V. Comparison With Measurements

The influence of the end ring leakage inductance, calculated by the 3D approach, is examined using a two dimensional finite element analysis by including or neglecting it in the analysis.

A. Combined finite element - circuit model

The outline of the finite element model is shown in figure 6. As the number of slots per pole is an integer, it is sufficient to model only one pole, and apply the appropriate boundary conditions. The analysis includes saturation using an iterative proces of both static (non-linear) and time-harmonic (linear) solutions [4]. Instead of using an effective magnetisation characteristic to obtain the reluctivities, the reluctivities are calculated based on two static solutions. From a time-harmonic solution, real and imaginary part of both stator- and rotor currents are extracted. These currents are used as excitation for two static problems. The reluctivity in each element required for the next time-harmonic solution, is computed as the average reluctivity obtained from both static solutions. This proces is found to be very robust for both current driven or voltage driven calculations in all load situations, but requires longer computation time compared to the method of effective reluctivities that only uses a time-harmonic solution [5].

The motor end effects are included as lumped parameters external to the finite element model. Figure 13 shows the layout of the coupled finite element - circuit model used.

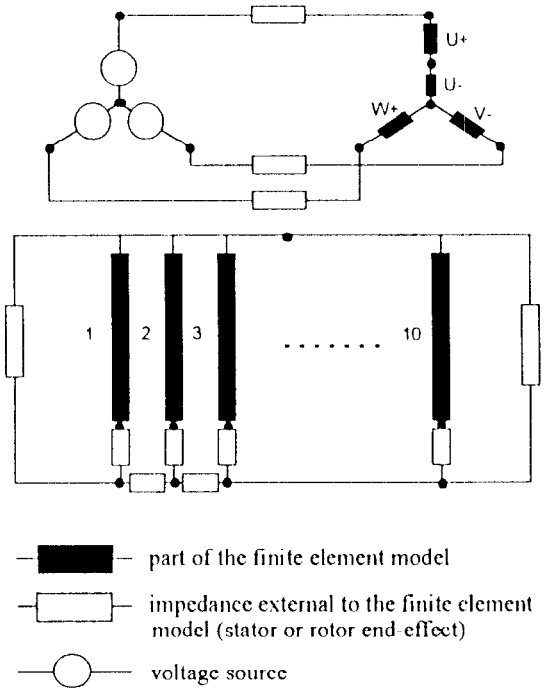

Fig. 13: Layout of the coupled finite element - circuit model, the labels are as shown in figure 6

The excitation for the two dimensional analysis is voltage driven (figure 13). The impedances between the three phase, Y-connected voltage source and the stator winding in the finite element model are the stator end winding leakage inductanc L_s and the end

winding resistance. The rotor circuit is described with a common node for all rotor bars (1 to 10). Therefore, the impedance modeled between two adjacent bars is equal to twice the impedance of a ring segment. The impedance in serie with each bar takes into account that the rotor bars are somewhat longer than the iron core.

To analyse the influence of both end winding and end ring inductance, three calculations are performed both for rated conditions and at standstill.

calculation 1: End ring and end winding leakage are ignored
calculation 2: Inclusion of the end winding leakage inductance
calculation 3: Both leakage inductances included.

B. Comparison with measurements at rated conditions

Table 2 shows the calculation results together with measurement data at rated conditions.

Table 2: Comparison of measurements and calculations at rated conditions

	Supply power [kW]	Stator current [A]
measurement	445.6	154.38
calculation 1	461.3	157.9
calculation 2	447.0	155.9
calculation 3	444.4	155.8

As can be seen from table 2, a small influence (< 2 %) of the end winding leakage is noticed. The influence of the end ring leakage is negligible: no significant variation of the solution is noticed.

C. Comparison with measurements at standstill

At standstill, the same calculations are performed, the supply voltage is reduced in order to obtain the rated stator current. Using the above described procedure to include saturation, it is noticed that the motor behaviour is linear. Therefore, a single time-harmonic solution is sufficient at standstill. Table 3 shows the calculation results together with measured data.

Table 3: Comparison of measurements and calculations at standstill

	Supply power [kW]	Inductance [mH]	Stator current [A]
measurement	14.30	3.18	153.97
calculation 1	19.1	2.7	174.8
calculation 2	15.9	3.0	161.5
calculation 3	14.3	3.2	152.9

The inductance in table 3 is calculated from the supply power P, the stator current I and the phase voltage V using

$$L = \frac{1}{\omega}\sqrt{\left(\frac{V}{I}\right)^2 - \left(\frac{P}{3I^2}\right)^2} \qquad (7)$$

with ω the supply pulsation. The calculation results at standstill show a significant influence of both end winding and end ring leakage inductance. Neglecting both leakage component results in an error larger than 15 % with the measured values, neglecting only the end ring leakage,the error is larger than 5 %.

D. Influence of the motor geometry.

Obviously, the influence of the motor end effects decreases when the length of the iron core increases. Also the rotor slot geometry has a distinct influence on the importance of the motor end leakage components. Similar calculations on traction motors having closed rotor slots show that the influence of the end winding and end ring leakage becomes much smaller in comparison with motors with open slots, even when the motors with closed slots are shorter than the motors with open rotor slots. This is explained by the fact that the motors with closed slots have an additional leakage component, the bridge leakage. This leakage component increases the overall leakage considerably [11]. Because this leakage component is strongly saturation dependent, it's influence has to be examined for each operating point separately.

VI. Conclusions

The ring inductance of a squirrel-cage induction motor is calculated using an analytical, a 2D and a 3D finite element approximation. The 2D approach is shown to be very useful for analysing the influence of the different materials in the end region by applying different boundary conditions. To separate the leakage part of the ring inductance, a 3D approach is required. The end winding and end ring leakage are shown to be strongly dependent on the load conditions. Both components are shown to decrease with increasing load, while the mutual inductance between end winding and end ring increases. The importance of both end winding and end ring inductance is shown by including or neglecting the components in the calculations and comparing the results with measured data. Both rated conditions and standstill are examined. The end ring inductance is shown to have significant influence at standstill, but is negligible at rated conditions.

Acknowledgment

The authors express their gratitude to the Belgian Ministry of Scientific Research for granting the IUAP No. 51 on Magnetic Fields, to Holec, Machines & Apparaten, Ridderkerk and to the Council of the Belgian National Science Foundation.

References

[1] A. Arkkio: "Finite element analysis of cage induction motors fed by static frequency convertors," *IEEE Trans. on Magnetics*, Vol. 26, No. 2, 1990, pp. 551-554.

[2] J. Luomi, A. Niemenmaa, A. Arkkio: "On the use of effective relucivities in magnetic field analysis of induction motors fed from a sinusoidal voltage source," *Proc. ICEM München*, pp. 706-709, 1986.

[3] E. Vassent, G. Meunier, J.C. Sabonnadiere: "Simulation of induction machine operation using complex magnetodynamic finite elements", *IEEE Trans. on Magnetics*, Vol. 25, No. 4, 1989, pp. 3064-3066.

[4] Belmans R., De Weerdt R., and Tuinman E.: "Combined field analysis techniques and macroscopic parameter simulation for describing the

behaviour of medium sized squirrel-cage induction motors fed with an arbitrary voltage," *EPE Brighton*, Sept. 1993, pp. 413-418.

[5] De Weerdt R., Brandiski K., Pahner U. and Belmans R.: "Comparative analysis of two methods for time-harmonic solution of the steady state in induction motors," *J. Appl. Phys.* 75 (10), Proc. of the 38th Annual Conference on Magnetism and Magnetic Materials, p. 6050.

[6] Nürnberg W.: *Die Asynchronmaschine*, Springer Verlag Berlin Heidelberg New York, 1952.

[7] Liwschitz-Garik: *Alternating Current Machines*, D. Van Nostrand Company, Ltd. 1946.

[8] S. Williamson, M.A. Mueller: "Calculation of the impedance of rotor cage end rings", *IEE Proc.* Vol. 140, Pt. B, No. 1, 1993, pp. 51-60.

[9] E.M. Freeman: *MagNet User Guide*, Infolytica Montreal, 1994.

[10] A.Lowther, P.P.Silvester: *Computer-Aided Design in Magnetics*, Springer-Verlag, New York, 1985.

[11] S. Wiliamson, M.C. Begg: "Calculation of the bar resistance and leakage reactance of cage rotors with closed slots", *IEE Proc.* Vol. 132, Pt. B, No. 3, 1985, pp. 125-132.